Supplementary Material: Quantum Entanglement Distribution via Uplink Satellite Channels

S. Srikara[1], Hudson Leone[1], Alexander Solnstev[2], and Simon J. Devitt[1,3]

[1]Center for Quantum Software and Information, University of Technology Sydney, NSW 2007, Australia
[2]School of Mathematical and Physical Sciences, University of Technology Sydney, Ultimo, NSW, 2007, Australia
[3]InstituteQ, Aalto University, 02150 Espoo, Finland.

1 Introduction

We are exploring an Entanglement-Swapping protocol for generating a Bell-pair between two ground stations using a satellite via uplink transmission. In this appendix, we derive the expressions for (a) the fidelity of the final bell state between the two ground stations and (b) the success probability (which is equivalent to the dual-channel efficiency) of the protocol.

2 Setup

The setup consists of two ground stations separated by a distance D_G and a satellite present in space above the two ground stations (Figure 1). Each ground station consists of a Bell-pair generator which generates perfect (i.e. fidelity 1) Bell-pairs of which at least one of the qubits (i.e. at least the one to be sent to the satellite) is a polarization-encoded photon. At the satellite, we have two receiving telescopes, one for each mode (i.e. one for receiving from each ground station) that captures the incoming photons and sends them to the Bell measurement apparatus (Figure 2). The apparatus consists of a polarizing beamsplitter (PBS) followed by an optical Hadamard (i.e. a 45° polarizer) and two polarization-resolving photon detectors. Each polarization-resolving photon detector is itself made of a polarizing beamsplitter followed by two photodetectors. The protocol occurs as follows:

1. A Bell-pair (in which at least one of the qubits of the pair is a polarization-encoded photon) is simultaneously generated at both the ground stations.
2. One (photonic) qubit of the Bell-pair from each ground station is sent toward the satellite while the other qubit is retained at the ground.
3. The photons reach the satellite simultaneously and undergo a Bell measurement on the satellite, causing entanglement swapping, thus leading to a newly-formed Bell-pair shared between the two ground-stations.

In step 2, the traveling photons are subject to several losses (Sections 4 and 5) and noisy stray light (Section 6) during travel, which has a significant impact on the fidelity and success probability of the protocol.

3 Calculation of Fidelity and Dual-Channel efficiency

During a photon's journey from ground to satellite (uplink), it is subject to several losses occurring from beam widening, beam wandering, and atmosphere 5. Once both photons complete their journey, they need to undergo Bell-measurement(s), where there will be some loss due to the inefficiency of the measurement apparatus, corrupted measurements due to stray photons 6, and a mismatch in the spatio-temporal modes of the photonic wavepackets as the photons may not be incident simultaneously on the measurement apparatus. In this appendix, we model these factors and derive the expression for the fidelity and success probability of these protocols. We ignore polarization error [7, 15] and Doppler effect [25, 16] as they are negligible.

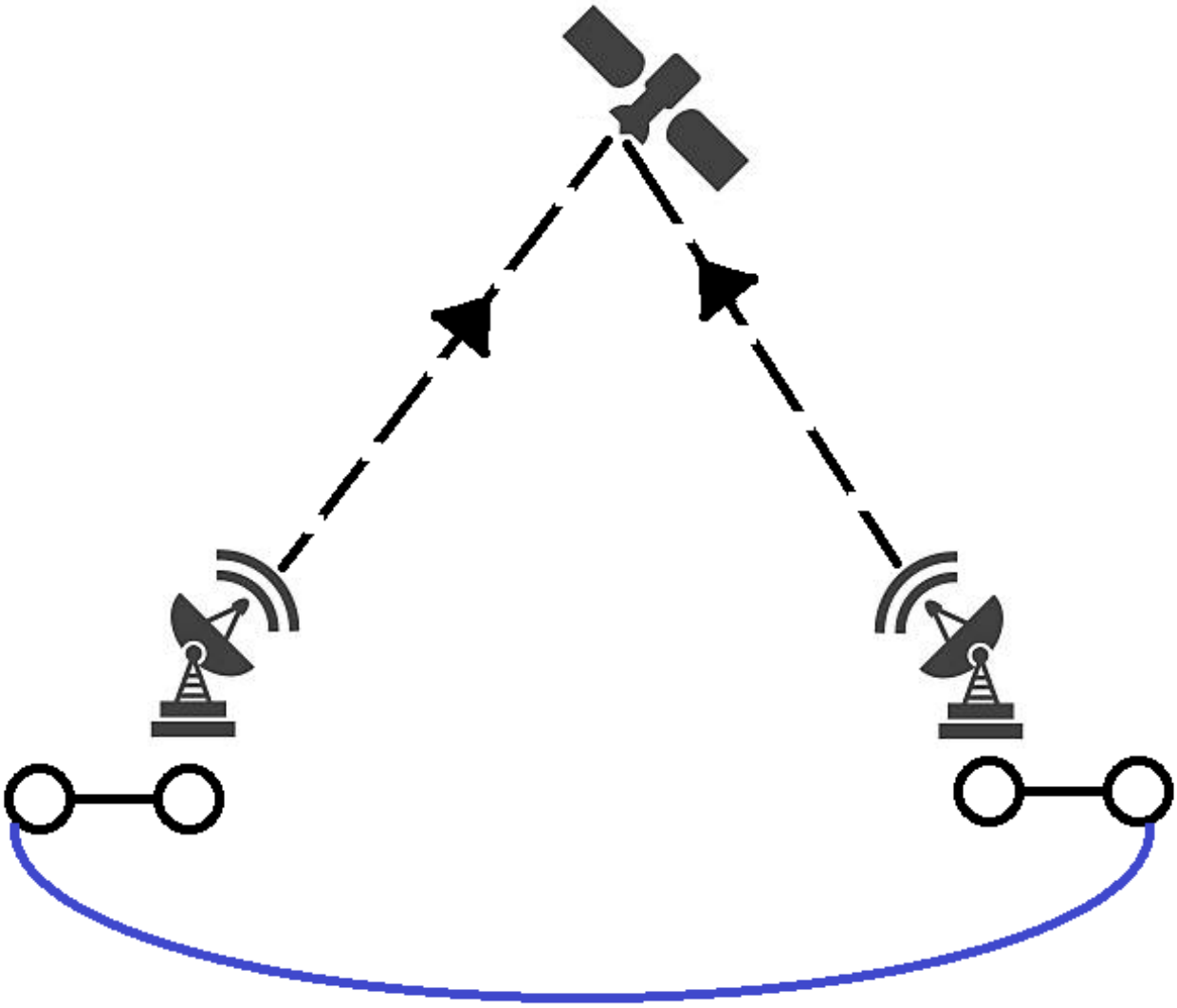

Figure 1: A schematic of the the proposed uplink setup. The setup consists of two ground stations sending one-half of their Bell pairs to a satellite via an uplink channel. The Bell measurement happens on the satellite, entangling the other two ground photons (represented by the dark blue curvy line).

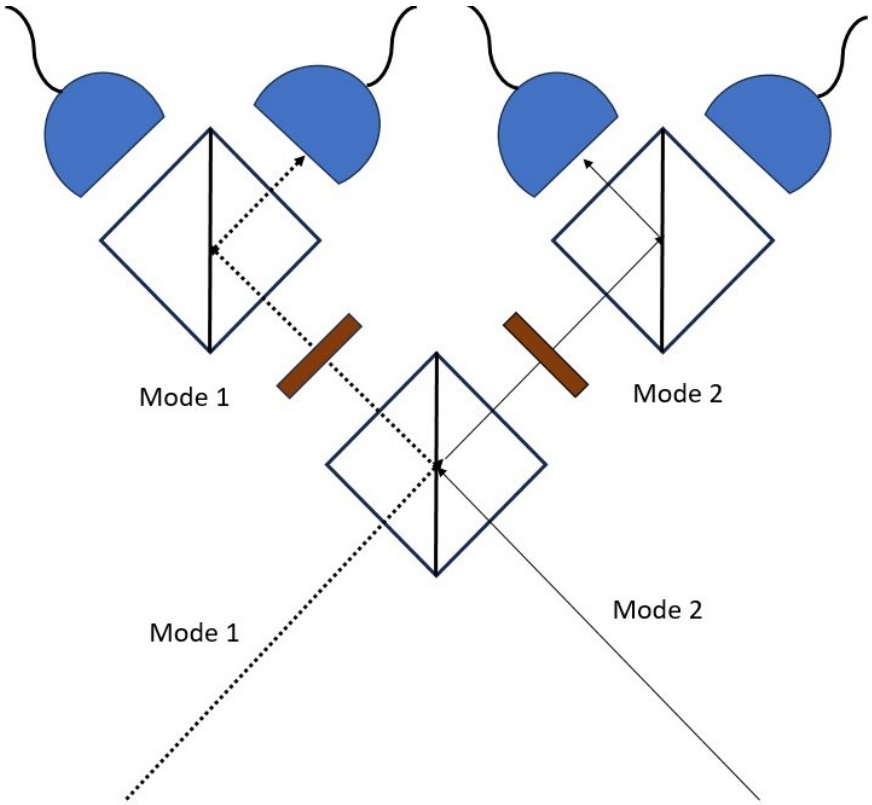

Figure 2: Bell Measurement setup inside the satellite. The setup consists of a polarizing beamsplitter (PBS) followed by two 45° polarizers (colored brown) followed by two polarization-resolving detectors, which themselves are made up of a PBS and two photodetectors each (in blue). This particular case shows an HH measurement result.

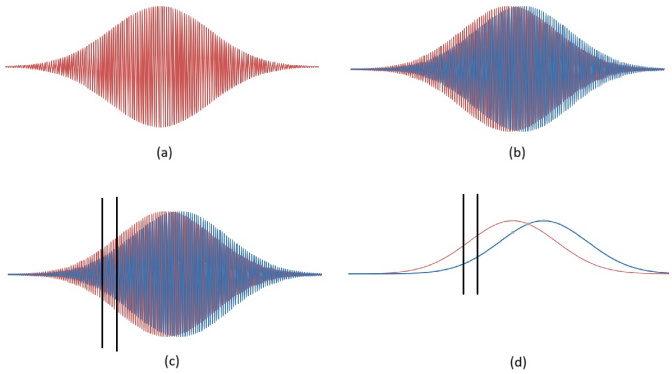

Figure 3: (a) A Gaussian wavepacket associated with a photon. (b) Mode mismatch between two wavepackets, increasing their distinguishability. (c) Time-gating between the two wavepackets, reducing their distinguishability but (d) lowering their detection probability as given by the normal distribution $|\psi(x)|^2$

4 Mode Mismatch

In this section we are assuming that all other effects (such as beam widening, wandering, stray photons, etc.) are all switched off and mode-mismatch is the only effect in play.

Every photon has a probability wavepacket ψ associated with it such that $|\psi|^2$ becomes the probability density function of the photon's position (Figure 3). During optical bell measurements, it is important that the two incoming photons arrive at the satellite simultaneously i.e. the wavepackets of the two incoming photons should spatiotemporally align. We call this mode-matching [23, 24]. Any spatiotemporal mismatch between the two wavepackets leads to increased distinguishability between the two photons, thus leading to reduced fidelity of the swapped bell pairs on the ground. To mitigate this, we employ a time-gating window i.e. a short, limited time window when the photon detectors are on. This allows only a fraction of the wavepackets to be detected, thus decreasing their distinguishability but at the same time reducing the probability of successful measurement. Therefore, the choice of the length of the gating window depends upon how much fidelity and measurement-success-probability is desired.

Although we are considering the halves of the Bell-pairs at the ground to be of arbitrary architectures, we can, without loss of generality, consider them to be photonic as well, for the purposes of our analysis.

A photon in free space located at position x_0 is described by the Gaussian wavepacket ψ (Figure 3) centred at x_0, given by [20]:

$$\psi(x) = \left(\frac{1}{2\pi\sigma^2}\right)^{\frac{1}{4}} e^{-\frac{1}{4}\left(\frac{x-x_0}{\sigma}\right)^2} e^{ik(x-x_0)},\ \sigma = c\sigma_t \tag{1}$$

where σ_t is the temporal width of the wavepacket and $k = 2\pi/\lambda$ is the wave number (where λ is the wavelength of the ground photon) and c is the speed of light.

Consider the two incoming photons from the two ground stations whose associated wavepackets are ψ_1 and ψ_2 respectively. Let's say these photons are incident on the satellite at times t_1 and t_2. This leads to a temporal mismatch $\Delta t = t_2 - t_1$ between the two photons, which can also be interpreted as the path difference Δx, such that $\Delta x = c\Delta t$ and therefore $\psi_2(x) = \psi_1(x + \Delta x)$. Here we are considering both photons to have the same σ_t as similar wavepacket configurations maximise overlap, which in turn maximises fidelity.

Figure 1 shows the uplink transmission. Without loss of generality, let us consider the initial states at the two ground stations to be polarization-encoded Bell-states $|HH\rangle + |VV\rangle$ at both places. Let's label the optical mode corresponding to the photon coming from ground station A as mode 1 and the optical mode corresponding to the photon coming from ground station B as mode 2. The state is (Let's defer normalization to the end):

$$|\Psi\rangle = \frac{1}{2}(|HH_1\rangle + |VV_1\rangle) \otimes (|H_2H\rangle + |V_2V\rangle) \tag{2}$$

Now, taking this system and factorizing out the two polarisation-encoded qubits (of mode 1 and 2) on which the bell measurement will be made, we have:

$$|\Psi\rangle = \frac{1}{2}(|HH\rangle\,|H\rangle_1\,|H\rangle_2 + |HV\rangle\,|H\rangle_1\,|V\rangle_2 + |VH\rangle\,|V\rangle_1\,|H\rangle_2 + |VV\rangle\,|V\rangle_1\,|V\rangle_2) \tag{3}$$

where the subscripts 1 and 2 refer to optical modes 1 and 2 respectively.
We represent the photonic states using mode operators,

$$\begin{aligned}\hat{H}_i^\dagger(\psi) &= \int \psi(x)\hat{h}_i^\dagger(x)dx,\\ \hat{V}_i^\dagger(\psi) &= \int \psi(x)\hat{v}_i^\dagger(x)dx,\end{aligned} \tag{4}$$

where i denotes optical mode and $\hat{h}^\dagger(x)/\hat{v}^\dagger(x)$ denote the horizontal and vertical photonic creation operators at time t. We assume all integrals run over the range $[-\infty,\infty]$ and that the photonic wavefunctions are normalised,

$$\int |\psi(x)|^2 dx = 1. \tag{5}$$

Then our net state is of the form,

$$\begin{aligned}|\Psi\rangle = \frac{1}{2}\Big(&|HH\rangle\,\hat{H}_1^\dagger(\psi_1)\hat{H}_2^\dagger(\psi_2)\,|0,0\rangle + |HV\rangle\,\hat{H}_1^\dagger(\psi_1)\hat{V}_2^\dagger(\psi_2)\,|0,0\rangle\\ &+ |VH\rangle\,\hat{V}_1^\dagger(\psi_1)\hat{H}_2^\dagger(\psi_2)\,|0,0\rangle + |VV\rangle\,\hat{V}_1^\dagger(\psi_1)\hat{V}_2^\dagger(\psi_2)\,|0,0\rangle\Big)\end{aligned} \tag{6}$$

where $|0,0\rangle$ is the vacuum state of the dual fock space and is not to be confused with the qubit notations of $|0\rangle$ and $|1\rangle$. The polarising beamsplitter transformation $\hat{U}_{\text{PBS}}$ implements,

$$\begin{aligned}\hat{H}_1^\dagger(\psi) &\to \hat{H}_1^\dagger(\psi),\\ \hat{H}_2^\dagger(\psi) &\to \hat{H}_2^\dagger(\psi),\\ \hat{V}_1^\dagger(\psi) &\to \hat{V}_2^\dagger(\psi),\\ \hat{V}_2^\dagger(\psi) &\to \hat{V}_1^\dagger(\psi),\end{aligned} \tag{7}$$

Applying this to our state yields,

$$\begin{aligned}\hat{U}_{\text{PBS}}\,|\Psi\rangle = \frac{1}{2}\Big(&|HH\rangle\,\hat{H}_1^\dagger(\psi_1)\hat{H}_2^\dagger(\psi_2)\,|0,0\rangle + |HV\rangle\,\hat{H}_1^\dagger(\psi_1)\hat{V}_1^\dagger(\psi_2)\,|0,0\rangle\\ &+ |VH\rangle\,\hat{V}_2^\dagger(\psi_1)\hat{H}_2^\dagger(\psi_2)\,|0,0\rangle + |VV\rangle\,\hat{V}_2^\dagger(\psi_1)\hat{V}_1^\dagger(\psi_2)\,|0,0\rangle\Big)\end{aligned} \tag{8}$$

The terms $|HV\rangle\,\hat{H}_1^\dagger(\psi_1)\hat{V}_1^\dagger(\psi_2)\,|0,0\rangle$ and $|VH\rangle\,\hat{V}_2^\dagger(\psi_1)\hat{H}_2^\dagger(\psi_2)\,|0,0\rangle$ are the terms indicating both photons travelling in the same mode after the action of PBS. These terms don't lead to two-mode clicks. Therefore, we discard them. This yields,

$$\hat{U}_{\text{PBS}}\,|\Psi\rangle = \frac{1}{2}\Big(|HH\rangle\,\hat{H}_1^\dagger(\psi_1)\hat{H}_2^\dagger(\psi_2)\,|0,0\rangle + |VV\rangle\,\hat{V}_1^\dagger(\psi_2)\hat{V}_2^\dagger(\psi_1)\,|0,0\rangle\Big) \tag{9}$$

Now, both the photons go through the 45° waveplates $\hat{U}_{wp_i}$ at each mode $i \in 1,2$ which perform hadamard transforms as follows:

$$\begin{aligned}\hat{H}_i^\dagger(\psi) &\to \frac{1}{\sqrt{2}}(\hat{H}_i^\dagger(\psi) + \hat{V}_i^\dagger(\psi)),\\ \hat{V}_i^\dagger(\psi) &\to \frac{1}{\sqrt{2}}(\hat{H}_i^\dagger(\psi) - \hat{V}_i^\dagger(\psi))\end{aligned} \tag{10}$$

The resulting state after these two Hadamard transformations is,

$$\begin{aligned}(\hat{U}_{wp_1}\otimes\hat{U}_{wp_2})\hat{U}_{\text{PBS}}\,|\Psi\rangle = \frac{1}{4}\Big(&|HH\rangle\,(\hat{H}_1^\dagger(\psi_1) + \hat{V}_1^\dagger(\psi_1))(\hat{H}_2^\dagger(\psi_2) + \hat{V}_2^\dagger(\psi_2))\,|0,0\rangle\\ &+ |VV\rangle\,(\hat{H}_1^\dagger(\psi_2) - \hat{V}_1^\dagger(\psi_2))(\hat{H}_2^\dagger(\psi_1) - \hat{V}_2^\dagger(\psi_1))\,|0,0\rangle\Big)\end{aligned} \tag{11}$$

Next we apply time-gating on both modes with time-gating, implementing the projector on each mode,

$$\begin{aligned}\hat{T}_i(\tau) &= \int \tau(t)\hat{a}_i^\dagger(t)\left|0\right\rangle\left\langle 0\right|\hat{a}_i(t)dt \\ &= \int c\tau(t)\hat{a}_i^\dagger(x(t))\left|0\right\rangle\left\langle 0\right|\hat{a}_i(x(t))dx \end{aligned} \tag{12}$$

where c is the speed of light, $\hat{a}^\dagger$ takes the polarisation in which the projection takes place and $\tau(t)$ is a window function ($\tau(t)=0$ when the gate is closed at t and $\tau(t)=1$ when open). Assuming that $\tau(t)$ is a top hat function bounded by $t_{\min}$ and $t_{\max}$, $c\tau(t)$ has the effect of limiting the bounds on the integrals between $ct_{\min}$ and $ct_{\max}$. Since we are looking at the wavepackets from photon perspe Upon performing a Hadamard transform on both qubits and measuring a HH coincidence click (with analogous form for the other outcomes), expanding the integrals we obtain,

$$\begin{aligned}\left|\phi\right\rangle = (\hat{T}_\tau^{(1)}\otimes\hat{T}_\tau^{(2)})\hat{U}_{\text{PBS}}\left|\Psi\right\rangle = \frac{1}{2}\Bigg(&\left|HH\right\rangle\int_{ct_{\min}}^{ct_{\max}}\int_{ct_{\min}}^{ct_{\max}}\psi_1(x_1)\psi_2(x_2)\hat{h}_1^\dagger(x_1)\hat{h}_2^\dagger(x_2)dx_1dx_2\left|0,0\right\rangle \\ &+(-1)^p\left|VV\right\rangle\int_{ct_{\min}}^{ct_{\max}}\int_{ct_{\min}}^{ct_{\max}}\psi_2(x_1)\psi_1(x_2)\hat{h}_1^\dagger(x_1)\hat{h}_2^\dagger(x_2)dx_1dx_2\left|0,0\right\rangle\Bigg)\end{aligned} \tag{13}$$

where the sign in the superposition is determined by the parity p of the measurement outcomes. $p=0$ for HH and VV outcomes, and $p=1$ for HV and VH outcomes.

Expressing the above as a density matrix we have,

$$\begin{aligned}\hat{\rho} &= \left|\phi\right\rangle\!\left\langle\phi\right| \\ &= \frac{1}{4}\Bigg(\left|HH\right\rangle\left\langle HH\right|\Bigg[\int_{ct_{\min}}^{ct_{\max}}\int_{ct_{\min}}^{ct_{\max}}\psi_1(x_1)\psi_2(x_2)\hat{h}_1^\dagger(x_1)\hat{h}_2^\dagger(x_2)dx_1dx_2\left|0,0\right\rangle \\ &\left\langle 0,0\right|\int_{ct_{\min}}^{ct_{\max}}\int_{ct_{\min}}^{ct_{\max}}\psi_1^*(x_1)\psi_2^*(x_2)\hat{h}_1(x_1)\hat{h}_2(x_2)dx_1dx_2\Bigg] \\ &+(-1)^p\left|HH\right\rangle\left\langle VV\right|\Bigg[\int_{ct_{\min}}^{ct_{\max}}\int_{ct_{\min}}^{ct_{\max}}\psi_1(x_1)\psi_2(x_2)\hat{h}_1^\dagger(x_1)\hat{h}_2^\dagger(x_2)dx_1dx_2\left|0,0\right\rangle \\ &\left\langle 0,0\right|\int_{ct_{\min}}^{ct_{\max}}\int_{ct_{\min}}^{ct_{\max}}\psi_2^*(x_1)\psi_1^*(x_2)\hat{h}_1(x_1)\hat{h}_2(x_2)dx_1dx_2\Bigg] \\ &+(-1)^p\left|VV\right\rangle\left\langle HH\right|\Bigg[\int_{ct_{\min}}^{ct_{\max}}\int_{ct_{\min}}^{ct_{\max}}\psi_2(x_1)\psi_1(x_2)\hat{h}_1^\dagger(x_1)\hat{h}_2^\dagger(x_2)dx_1dx_2\left|0,0\right\rangle \\ &\left\langle 0,0\right|\int_{ct_{\min}}^{ct_{\max}}\int_{ct_{\min}}^{ct_{\max}}\psi_1^*(x_1)\psi_2^*(x_2)\hat{h}_1(x_1)\hat{h}_2(x_2)dx_1dx_2\Bigg] \\ &+\left|VV\right\rangle\left\langle VV\right|\Bigg[\int_{ct_{\min}}^{ct_{\max}}\int_{ct_{\min}}^{ct_{\max}}\psi_2(x_1)\psi_1(x_2)\hat{h}_1^\dagger(x_1)\hat{h}_2^\dagger(x_2)dx_1dx_2\left|0,0\right\rangle \\ &\left\langle 0,0\right|\int_{ct_{\min}}^{ct_{\max}}\int_{ct_{\min}}^{ct_{\max}}\psi_2^*(x_1)\psi_1^*(x_2)\hat{h}_1(x_1)\hat{h}_2(x_2)dx_1dx_2\Bigg]\Bigg)\end{aligned} \tag{14}$$

Next we trace out the two detected optical modes as all remaining temporal information is inaccessible to us,

$$
\begin{aligned}
\hat{\rho}_{mm} &= \mathrm{tr}_{1,2}(\hat{\rho}) \\
&= \frac{1}{4}\Bigg(|HH\rangle\langle HH| \left[\int_{ct_{\min}}^{ct_{\max}} |\psi_1(x)|^2 dx \int_{ct_{\min}}^{ct_{\max}} |\psi_2(x)|^2 dx\right] \\
&+ (-1)^p |HH\rangle\langle VV| \left[\left|\int_{ct_{\min}}^{ct_{\max}} \psi_1(x)\psi_2^*(x) dx\right|^2\right] \\
&+ (-1)^p |VV\rangle\langle HH| \left[\left|\int_{ct_{\min}}^{ct_{\max}} \psi_1(x)\psi_2^*(x) dx\right|^2\right] \\
&+ |VV\rangle\langle VV| \left[\int_{ct_{\min}}^{ct_{\max}} |\psi_1(x)|^2 dx \int_{ct_{\min}}^{ct_{\max}} |\psi_2(x)|^2 dx\right]\Bigg)
\end{aligned} \tag{15}
$$

Let,

$$
\begin{aligned}
\zeta &= \int_{ct_{\min}}^{ct_{\max}} |\psi_1(x)|^2 dx \int_{ct_{\min}}^{ct_{\max}} |\psi_2(x)|^2 dx, \\
\gamma &= \left|\int_{ct_{\min}}^{ct_{\max}} \psi_1(x)\psi_2^*(x) dx\right|^2.
\end{aligned} \tag{16}
$$

Then,

$$
\hat{\rho}_{mm} = \mathrm{tr}_{1,2}(\hat{\rho}) = \frac{1}{4}\Big(\zeta |HH\rangle\langle HH| + (-1)^p\gamma |HH\rangle\langle VV| + (-1)^p\gamma |VV\rangle\langle HH| + \zeta |VV\rangle\langle VV|\Big) \tag{17}
$$

Then, the probability P_{gw} that the photon entering mode i passes through the gating window is given by,

$$
P_{gw_i} = \int_{ct_{\min}}^{ct_{\max}} |\psi_i(x)|^2 dx \tag{18}
$$

where $i = 1$ for photon from ground station A and $i = 2$ for photon from ground station B. Thus, $\zeta = P_{gw_1}P_{gw_2}$. For an ideal parity projection we expect the state after normalisation,

$$
|\Phi\rangle = \frac{1}{\sqrt{2}}(|HH\rangle + (-1)^p |VV\rangle) \tag{19}
$$

The fidelity F_{ic} (under ideal channel assumptions) between the actual and expected states is given by,

$$
F_{ic} = \frac{\langle\Phi|\hat{\rho}_{mm}|\Phi\rangle}{\mathrm{tr}(\hat{\rho}_{mm})} = \frac{1}{2} + \frac{\gamma}{2P_{gw_1}P_{gw_2}} \tag{20}
$$

5 Channel Errors

5.1 Geometries

Before we consider the channel errors (Figure 4), let's first define some prerequisite trigonometries that relate to the positions of the satellites and ground stations (Figure 5). Consider the ground station A. Let h be the satellite altitude. Let θ be the zenith angle at the ground station i.e. the angle between the vertical above the ground station and the line connecting the ground station to the satellite. Let $z(h,\theta)$ be the distance between the ground station and the satellite. Let α be the angle between the line that connects the ground station to the earth's center and the line that connects the satellite to the earth's center. Let E_R be the earth's radius. Let θ_2, $z_2(h,\theta_2)$, and α_2 be the corresponding parameters for ground station B. Let D_G be the on-ground distance of separation between the two ground stations. For our analysis, we assume that the ground stations A and B, along with the satellite, and the point at the center of Earth, are all in the same plane. Then $z(h,\theta)$ is given by [21]:

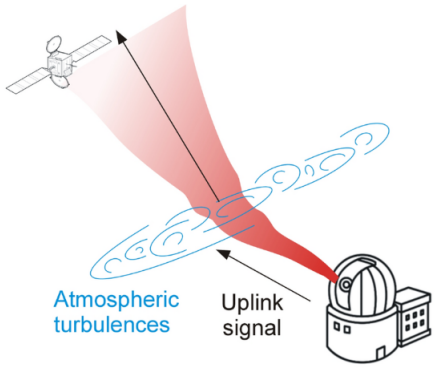

Figure 4: Photon beam profile due to beam widening, beam wandering, and atmospheric turbulence [1].

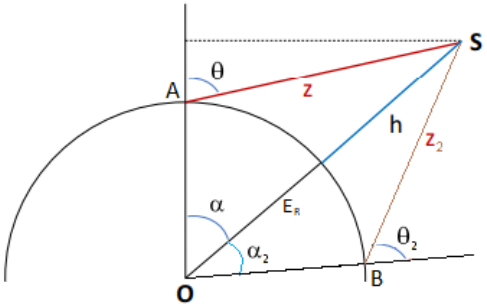

Figure 5: Geometries of the setup. A and B are the ground stations, O is the center of the earth, and S is the satellite.

$$z(h,\theta) = \sqrt{h^2 + 2hE_R + E_R^2\cos^2\theta} - E_R\cos\theta \tag{21}$$

rearranging the terms, we get the expression for h:

$$h(z,\theta) = \sqrt{E_R^2 + z^2 + 2zE_R\cos\theta} - E_R \tag{22}$$

The same z can also be represented as a function of α in such a way that:

$$z(h,\alpha) = \sqrt{E_R^2 + (E_R+h)^2 - 2E_R(E_R+h)\cos\alpha} \tag{23}$$

α and θ are related by:

$$\alpha(h,\theta) = \cos^{-1}\left[\frac{E_R + z(h,\theta)\cos\theta}{E_R+h}\right] \iff \theta(h,\alpha) = \cos^{-1}\left[\frac{(E_R+h)\cos\alpha - E_R}{z(h,\alpha)}\right] \tag{24}$$

For the second ground station, α_2 is given by:

$$\alpha_2 = \frac{D_G}{E_R} - \alpha \tag{25}$$

Using the above relations, θ_2 and z_2 can be determined.

In a special case where the satellite is located symmetrically equidistant from both ground stations, then the common zenith angle θ_e is given by:

$$\theta_e(h,D_G) = \cos^{-1}\left[\frac{(E_R+h)\cos\left(\frac{D_G}{2E_R}\right) - E_R}{z\left(h,\alpha = \frac{D_G}{2E_R}\right)}\right] \tag{26}$$

Here, we have substituted $\alpha = \alpha_2 = D_G/2E_R$ onto Eq. 24 to get Eq. 26

5.2 Errors Due to Beam Widening and Wandering

Beam widening and beam wandering phenomena affect channel efficiency in satellite communications [21, 8, 1]. Beam widening is a phenomenon where the width of the beam gradually increases with travel, making the overall beam conical [27, 2, 9, 26], while beam wandering is a phenomenon where the mean photon position in the beam (also called beam centroid in most literature [14, 21, 1]) randomly varies as it passes through the atmosphere due to changing refractive index of the atmosphere caused by turbulence. Beam wandering and beam widening errors are higher in uplink channels than downlink channels because in uplink the photons interact with the atmosphere right at the beginning of the journey, causing higher deviations in the photon trajectory compared to downlink.

For satellites located at height ranges of LEO (Low-Earth Orbit) and beyond, the overall long-term beam width w due to the combined effects of beam widening and wandering (not to be confused with the width σ of the probability wavepacket of the photons) is given by [21, 8]:

$$w^2 = w_0^2 \left(1 + \left(\frac{z\lambda}{\pi w_0^2}\right)^2\right) + 2\left(\frac{\lambda z}{\pi \kappa_0}\right)^2 \tag{27}$$

where:

$$\kappa_0 = \left[1.46\left(\frac{2\pi}{\lambda}\right)^2 (\sec(\theta)) C_w\right]^{-3/5} \tag{28}$$

where: where w_0 is the initial beam width, z is the distance between the ground station and the satellite i.e. the length of the path of photon travel, λ is the wavelength of the photon, and θ is the zenith angle i.e. the angle between the vertical and the line connecting the ground station to the satellite. Here, the first term is the beam widening term while the second term characterizes beam wandering due to atmospheric turbulence. The constant C_w takes the values $C_w = 2.2354 \times 10^{-12}\mathrm{m}^{1/3}$ during the night and $C_w = 3.2854 \times 10^{-12}\mathrm{m}^{1/3}$ during the day[21].

If R_A is the radius of aperture of the receiving telescope, then the average channel efficiency η_w due to beam widening and wandering (theoretically averaged a large number of repetitions) is given by [21, 8, 10]:

$$\eta_w = 1 - e^{-2R_A^2/(w^2 + 10^{-12}z^2 + \sigma_{\mathrm{tr}}^2)} \tag{29}$$

where $10^{-12}z^2$ is the pointing error of the transmitter [21] and σ_{tr} is the tracking error in Satellite's position.

5.3 Atmospheric Attenuation

The channel efficiency η_a resulting solely due to atmospheric attenuation is given by [21]:

$$\eta_a(h, \theta) = \exp\left[-\alpha_0 \int_0^{z(h,\theta)} exp\left[-\frac{h(y,\theta)}{\tilde{h}}\right] dy\right] \tag{30}$$

where h is the satellite altitude, $\alpha_0 = 5 \times 10^{-6} m^{-1}$ and $\tilde{h} = 6600m$ are constants [6, 30].

5.4 Overall Single-Photon Channel Efficiency

Let $\eta_m = \eta_{PBS}\eta_{wp}\eta_{PBS}\eta_{det}$ be the efficiency of the measurement apparatus, including detector efficiency η_{det}, the transmissivity of the PBSes η_{PBS}, waveplate η_{wp}, and detector efficiency η_{det}. Then, the total success probability η_A (η_B) of a single photon to travel from a ground station A (B) to the detector in the satellite and causes a detector click is given by:

$$\begin{aligned} \eta_A &= (\eta_w \times \eta_a)_{\mathrm{photon1}} \times \eta_m \times P_{gw_1} \\ \eta_B &= (\eta_w \times \eta_a)_{\mathrm{photon2}} \times \eta_m \times P_{gw_2} \end{aligned} \tag{31}$$

6 Stray Photons and Noise

Earth's blackbody radiation, moonlight, reflected sunlight, etc. contribute to numerous stray photons [13, 19, 17]. These stray photons, when incident on the measurement apparatus along with the legitimate photons, can lead to corrupted measurements. Corrupted measurements can be of several types. Two detector clicks arising due to one or more stray photons can't be distinguished from a legitimate double-click detection event happening purely due to the photons sent from the ground stations. This leads to false positive measurement results leading to reduced fidelity. More than two clicks arising due to stray photons lead to the discarding of that result, leading to lower channel efficiency.

During the daytime, the number of stray photons N_D per second per unit bandwidth incident on the satellite's receiving telescope is given by [8]:

$$N_D = EI_S R_A^2 \theta_{FOV}^2 \tag{32}$$

where E is Earth's albedo, I_S is the solar spectral irradiance at one astronomical unit, R_A is the radius of aperture of the receiving telescope, and θ_{FOV} is the field of view of the receiving telescope.

At night, the number of photons N_N per second per unit bandwidth incident on the satellite's receiving telescope is given by:

$$N_N = \pi I_{BB} R_A^2 \theta_{FOV}^2 + N_D M \left(\frac{r_M}{l_{ME}}\right)^2 \tag{33}$$

where M is moon's albedo, r_M is moon's radius, l_{ME} is the distance between moon and Earth, and IBB is the spectral radiance due to blackbody radiation, given by [8]:

$$I_{BB}(\lambda) = \frac{2c}{\lambda^4} \frac{1}{e^{\frac{pc}{\lambda k_B T}} - 1} \tag{34}$$

where here p is the Planck's constant, k_B is the Boltzmann constant, and T is Earth's temperature at the emitting region.

6.1 Stray Photon Rates

Finally, the uplink rate r_{day} and r_{night} of stray photons incident on the photodetectors during daytime and night time respectively, is given by:

$$\begin{aligned} r_{\text{day}} &= C_D + \frac{1}{2}\eta_a \eta_m N_D \Delta\lambda \\ r_{\text{night}} &= C_D + \frac{1}{2}\eta_a \eta_m N_N \Delta\lambda \end{aligned} \tag{35}$$

where $\Delta\lambda$ is the filter bandwidth of the receiving telescope and C_D is the inherent dark count rate of the photodetectors. We have two receiving telescopes for the photons coming from two different ground stations. Therefore, there will be a factor of 2. Since the stray photons are assumed to be of maximally mixed polarization, the probability that they will land on any one of the given 4 detectors is 1/4. Therefore, $(1/4) \times 2 = 1/2$ factor comes into play. Since these photons also undergo attenuation from the atmosphere and the measurement apparatus, we add η_a and η_m. Since the initial beam widths of these stray photons are arbitrary, we ignore this effect. Adding this effect will only further reduce stray photons and improve fidelity. Demonstrating reasonable fidelity by ignoring the beam widening and wandering effect on the stray photons will automatically mean greater feasibility when this effect is included onto them.

Within a time-gating window t of the detector (where $t = t_{\max} - t_{\min}$)(not to be confused with Δt which is the path difference between the two photonic wavepackets divided by c), the probability that n stray photons are incident on a single detector follows the Poissonian distribution:

$$P_{sp}(n) = \frac{(r_{\text{day/night}} t)^n e^{-r_{\text{day/night}} t}}{n!} \tag{36}$$

7 Dual Channel Efficiency

In this section, we calculate the dual-channel efficiency of the whole protocol i.e. the success probability of the protocol. Although we will derive the general expression here, in our simulations, we will assume that both ground stations are equidistant from the satellite, and have similar weather and lighting conditions. Therefore we assume similar channel errors and stray photons, and also similar shaped wavepackets.

In our measurement setup, we have four detectors 1, 2, 3, and 4 (taken from left to right in Figure 2). Let the tuple $d = (d_1, d_2, d_3, d_4)$ denote the detection outcomes, with $d_i \in \{0, 1\}$ for detector i, where 0 represents no click whereas 1 represents a click. Let G and D be length-four binary tuples that encode possible measurement outcomes for the four photodetectors. Let G correspond to legitimate detection events i.e. detection events purely due to the legitimate photons coming from ground stations A and B, and let D correspond to detection events from stray photons. The probability that photons from the ground stations cause detector clicks d is $P_G(d)$. The probability that stray photons will cause detector clicks d is $P_D(d)$. The measurement signature M is given by the bit-wise AND of bit-strings associated with G and D. The allowed legitimate signatures are $M = (1, 0, 1, 0)$, $(1, 0, 0, 1)$, $(0, 1, 1, 0)$, and $(0, 1, 0, 1)$.

Consider one success signature $M = (1, 0, 1, 0)$. Since the photodetectors cannot differentiate between legitimate photons and stray photons, this can occur in any of the following ways:

- $G = (1, 0, 1, 0)$ with any of the stray photon configurations $D = (0, 0, 0, 0)$, $D = (0, 0, 1, 0)$,$D = (1, 0, 0, 0)$, $D = (1, 0, 1, 0)$.
- Or for $G = (0, 0, 1, 0)$ with $D = (1, 0, 0, 0)$, $(1, 0, 1, 0)$.
- Or for $G = (1, 0, 0, 0)$ with $D = (0, 0, 1, 0)$, $(1, 0, 1, 0)$.
- Or for $G = (0, 0, 0, 0)$ with $D = (1, 0, 1, 0)$.

i.e., we just find all the bit-strings that satisfy $M = G$ AND D.

From the law of total probability [5], the probability P_M of this happening is,

$$\begin{aligned} P_M(1,0,1,0) & \\ &= P_G(1,0,1,0)[P_D(0,0,0,0) + P_D(0,0,1,0) \\ &+ P_D(1,0,0,0) + P_D(1,0,1,0)] \\ &+ P_G(0,0,1,0)[P_D(1,0,0,0) + P_D(1,0,1,0)] \\ &+ P_G(1,0,0,0)[P_D(0,0,1,0) + P_D(1,0,1,0)] \\ &+ P_G(0,0,0,0)P_D(1,0,1,0) \end{aligned} \tag{37}$$

To find out the P_G and P_D functions, we note the symmetry that both functions are invariant under permutations of their parameter, depending only on the Hamming weight of the argument bit-string i.e. for instance

$$\begin{aligned} P_G(1,0,1,0) &= P_G(1,0,0,1) \\ &= P_G(0,1,1,0) \\ &= P_G(0,1,0,1) \\ &= P_G(1,1,0,0) \\ &= P_G(1,0,1,0) \\ &= P_G(0,0,1,1) \\ &= P_G(|d| = 2) \end{aligned} \tag{38}$$

and so on, where $|d|$ is the sum of the 1's in a given tuple. The same holds for P_D as well.

Let η_A and η_B be the overall single-photon channel efficiencies (from Eq.31) of the uplink channels from ground stations A and B respectively. Then,

$$P_{G_0} = P_G(|d| = 0) = (1 - \eta_A)(1 - \eta_B), \tag{39}$$

is the probability of neither of the ground photons reaching the satellite, and

$$P_{G_1} = P_G(|d| = 1) = [\eta_A(1 - \eta_B) + \eta_B(1 - \eta_A)]\frac{1}{4} + \frac{1}{16}\eta_A\eta_B, \tag{40}$$

is the probability of one of the ground photons reaching the satellite, and

$$P_{G_2} = P_G(|d| = 2) = \frac{1}{8}\eta_A\eta_B, \tag{41}$$

is the probability of both the photons reaching the satellite.

Similarly for stray photons, we have:

$$P_{D_0} = P_D(|d| = 0) = [P_{sp}(0)]^4 \tag{42}$$

$$P_{D_1} = P_D(|d| = 1) = [P_{sp}(0)]^3[1 - P_{sp}(0)] \tag{43}$$

$$P_{D_2} = P_D(|d| = 2) = [P_{sp}(0)]^2[1 - P_{sp}(0)]^2 \tag{44}$$

where $P_{sp}(n)$ is the probability of n stray photons entering the satellite during the measurement window (6).

With the new terminology, Eq. 37 becomes:

$$P_M(1, 0, 1, 0) = P_{G_2}[P_{D_0} + 2P_{D_1} + P_{D_2}] + 2P_{G_1}[P_{D_1} + P_{D_2}] + P_{G_0}P_{D_2} \tag{45}$$

Assuming that the four detectors are equally configured, it can be verified that all the four legitimate signatures are symmetric i.e.:

$$\begin{aligned} P_M(1, 0, 1, 0) &= P_M(1, 0, 0, 1) \\ &= P_M(0, 1, 1, 0) \\ &= P_M(0, 1, 0, 1) \\ &= P_M(|d| = 2) \end{aligned} \tag{46}$$

Note that in case of a successful signature as any of those given in Eq. 46, there could be the possibility of a non-legitimate signature $P_G(|d| <= 1)$ corrupted by stray photons. Since we cannot detect this, we accept this as a success signature. This leads to reduced fidelity of the final entangled state. In cases where we have the failure signatures of one, three, or four coincidence clicks, or of two coincidence clicks on the detectors of the same optical mode, we discard it, which is analytically equivalent to channel attenuation, affecting the total success probability of our protocol. In cases where the legitimate photons and the stray photons fall on the same detector, the detection is considered successful and legitimate as the detectors cannot differentiate between legitimate and stray photons.

Therefore, the total probability η_{tot} of successful signature for any given photon pair coming from the ground stations is given by:

$$\eta_{tot} = 4P_M(1, 0, 1, 0) \tag{47}$$

which can be equivalently considered as the dual uplink channel efficiency. The factor of 4 is due to the 4 success signatures as given in Eq. 46

8 Final Fidelity

Let's consider the success signature $M = (1, 0, 1, 0)$. The probability P_{SM} of a legitimate coincidence given the success signature M is given by:

$$\begin{aligned} P_{SM}(1, 0, 1, 0) &= \frac{P_G(1, 0, 1, 0)[P_D(0, 0, 0, 0) + P_D(0, 0, 1, 0) + P_D(1, 0, 0, 0) + P_D(1, 0, 1, 0)]}{P_M(1, 0, 1, 0)} \\ &= \frac{P_{G_2}[P_{D_0} + 2P_{D_1} + P_{D_2}]}{P_M(1, 0, 1, 0)} \end{aligned} \tag{48}$$

Table 1: Simulation Parameters

Parameter	Symbol	Value	Reference
Detector Dark Count Rate	C_D	1500 Hz	[28]
Telescope Aperture Radius	R_A	0.75 m	[22]
Field of View	θ_{FOV}	10^{-5} rad	[21, 4]
Filter Bandwidth	$\Delta\lambda$	1 nm	[21, 8]
Wavelength of Light	λ	800 nm	[21]
Temperature	T	300 K (27°C)	
Initial Beam Width	w_0	2.5cm	[21]
Efficiency of the Measurement Apparatus	η_m	0.25	[28]
Phase Mismatch	Δt	3 ns	
Earth's Albedo	E	0.3	[8]
Solar Spectral irradiance	I_S	$4.61 \times 10^{27}\text{Hz}/m^3$	[8]
Moon's Radius	r_M	1737.4 km	
Moon's Albedo	M	0.14	
Earth-moon Distance	l_{ME}	3.633×10^8 m	

Considering all four successful signatures, we see that P_{SM} is equivalent in all four instances with equally valued numerators due to the fact that P_G, P_D, and P_M are all invariant under permutations of (d_1, d_2, d_3, d_4). Therefore, the probability P_S of the coincidence being legitimate given any successful signature is:

$$P_S = P_{SM} \tag{49}$$

In case of an unsuccessful coincidence, the measurement collapses the state to a maximally mixed state $I/4$.

Therefore, the resulting final entangled state ρ_{final} shared between the two ground stations at the end of the protocol is given by:

$$\rho_{final} = P_S \hat{\rho}_{mm} + (1 - P_S)\frac{I}{4} \tag{50}$$

where $\hat{\rho}_{mm}$ is obtained from Eq. 15. actual fidelity F of the resulting swapped Bell-pair is given by:

$$F = \langle\Phi| \hat{\rho}_{mm} |\Phi\rangle = P_S F_{ic} + (1 - P_S)/4 \tag{51}$$

where F_{ic} is that of Eq. 20 and $|\Phi\rangle$ is from Eq. 19.

9 Parameter Settings

For our simulations, we consider the following values as given in table.1. For our simulations, we consider realistic parameter values chosen from various experiments and industry standards. We set the aperture width of the satellite's receiving telescope to be 75 cm, [22] though we note that practical instances of dishes may range in size from 30cm to 2m [22]. Although photon scattering is minimised at infrared wavelengths, a typical commercial photodetector [28] has a maximum detection efficiency at around 700nm. To compromise, we set the wavelength of our photons at 800nm where detection efficiency is roughly 60%. We consider an earth temperature of 27°C. We assume a measurement efficiency of $0.91 \times 0.5 \times 0.91 \times 0.6 = 0.25$. This accounts for the two PBSes, which are assumed to each have a transmissivity of around 0.91 [29], the photodetector which has an efficiency of 0.6 at 800 nm [28], and the 45° waveplate has an efficiency of 0.5 from Malu's Law. Though it's possible to engineer photon wavepackets at virtually any width [11, 12, 3], experimental constraints limit the range of possible values we can choose from. The larger a wavepacket is, the longer the detection window needs to be open which increases the probability of receiving stray photons. The other constraint is the precision with which a satellite clock can be synchronized with the ground station clocks. This is because photon mode matching is impossible when the widths of the incoming wave-packets are smaller than the precision of clock synchronisation. Recent experimental results demonstrated a satellite clock synchronisation at a precision of just under 1 ns [18]. In the best-case scenario, the clock synchronization is the only cause of mode mismatch which would lead us to assume a maximum mismatch of 0.9 ns between the modes of the coincident wavepackets. For confidence, we fix this at a more conservative 3 ns.

References

[1] D Alaluf and JM Perdigues Armengol. Ground-to-satellite optical links: how effective is an uplink tip/tilt pre-compensation based on the satellite signal? *CEAS Space Journal*, pages 1–12, 2021.

[2] LC Andrews, WB Miller, and JC Ricklin. Geometrical representation of gaussian beams propagating through complex paraxial optical systems. *Applied optics*, 32(30):5918–5929, 1993.

[3] Vahid Ansari, Emanuele Roccia, Matteo Santandrea, Mahnaz Doostdar, Christof Eigner, Laura Padberg, Ilaria Gianani, Marco Sbroscia, John M Donohue, Luca Mancino, et al. Heralded generation of high-purity ultrashort single photons in programmable temporal shapes. *Optics express*, 26(3):2764–2774, 2018.

[4] Robert Bedington, Juan Miguel Arrazola, and Alexander Ling. Progress in satellite quantum key distribution. *npj Quantum Information*, 3(1):30, 2017.

[5] Dimitri Bertsekas and John N Tsitsiklis. *Introduction to probability*, volume 1. Athena Scientific, 2008.

[6] Craig F Bohren and Donald R Huffman. *Absorption and scattering of light by small particles*. John Wiley & Sons, 2008.

[7] Cristian Bonato, Markus Aspelmeyer, Thomas Jennewein, Claudio Pernechele, Paolo Villoresi, and Anton Zeilinger. Influence of satellite motion on polarization qubits in a space-earth quantum communication link. *Optics express*, 14(21):10050–10059, 2006.

[8] Cristian Bonato, Andrea Tomaello, Vania Da Deppo, Giampiero Naletto, and Paolo Villoresi. Feasibility of satellite quantum key distribution. *New Journal of Physics*, 11(4):045017, 2009.

[9] Max Born and Emil Wolf. *Principles of optics: electromagnetic theory of propagation, interference and diffraction of light*. Elsevier, 2013.

[10] JP Bourgoin, Evan Meyer-Scott, Brendon L Higgins, B Helou, Chris Erven, Hannes Huebel, B Kumar, D Hudson, Ian D'Souza, Ralph Girard, et al. A comprehensive design and performance analysis of low earth orbit satellite quantum communication. *New Journal of Physics*, 15(2):023006, 2013.

[11] Qian Cao, Jian Chen, Keyin Lu, Chenhao Wan, Andy Chong, and Qiwen Zhan. Sculpturing spatiotemporal wavepackets with chirped pulses. *Photonics Research*, 9(11):2261–2264, 2021.

[12] Daniel Cruz-Delgado, Stephanos Yerolatsitis, Nicolas K Fontaine, Demetrios N Christodoulides, Rodrigo Amezcua-Correa, and Miguel A Bandres. Synthesis of ultrafast wavepackets with tailored spatiotemporal properties. *Nature Photonics*, 16(10):686–691, 2022.

[13] Miao Er-Long, Han Zheng-fu, Gong Shun-sheng, Zhang Tao, Diao Da-Sheng, and Guo Guang-Can. Background noise of satellite-to-ground quantum key distribution. *New Journal of Physics*, 7(1):215, 2005.

[14] Ronald L Fante. Electromagnetic beam propagation in turbulent media. *Proceedings of the IEEE*, 63(12):1669–1692, 1975.

[15] Alessandro Fedrizzi, Rupert Ursin, Thomas Herbst, Matteo Nespoli, Robert Prevedel, Thomas Scheidl, Felix Tiefenbacher, Thomas Jennewein, and Anton Zeilinger. High-fidelity transmission of entanglement over a high-loss free-space channel. *Nature Physics*, 5(6):389–392, 2009.

[16] Mark T Gruneisen, Mark L Eickhoff, Scott C Newey, Kurt E Stoltenberg, Jeffery F Morris, Michael Bareian, Mark A Harris, Denis W Oesch, Michael D Oliker, Michael B Flanagan, et al. Adaptive-optics-enabled quantum communication: A technique for daytime space-to-earth links. *Physical Review Applied*, 16(1):014067, 2021.

[17] V Hansen. Spectral distribution of solar radiation on clear days: A comparison between measurements and model estimates. *Journal of Applied Meteorology and Climatology*, 23(5):772–780, 1984.

[18] Florian Kunzi and Oliver Montenbruck. Precise onboard time synchronization for leo satellites. *NAVIGATION: Journal of the Institute of Navigation*, 69(3), 2022.

[19] Ch Leinert, S Bowyer, LK Haikala, MS Hanner, MG Hauser, A-Ch Levasseur-Regourd, I Mann, K Mattila, WT Reach, W Schlosser, et al. The 1997 reference of diffuse night sky brightness. *Astronomy and Astrophysics Supplement Series*, 127(1):1–99, 1998.

[20] Konstantin Likharev. *Essential Graduate Physics, Part QM: Quantum Mechanics*. Stony Brook University, 2013.

[21] Stefano Pirandola. Satellite quantum communications: Fundamental bounds and practical security. *Physical Review Research*, 3(2):023130, 2021.

[22] Ji-Gang Ren, Ping Xu, Hai-Lin Yong, Liang Zhang, Sheng-Kai Liao, Juan Yin, Wei-Yue Liu, Wen-Qi Cai, Meng Yang, Li Li, et al. Ground-to-satellite quantum teleportation. *Nature*, 549(7670):70–73, 2017.

[23] Peter P Rohde and Timothy C Ralph. Frequency and temporal effects in linear optical quantum computing. *Physical Review A*, 71(3):032320, 2005.

[24] Peter P Rohde and Timothy C Ralph. Time-resolved detection and mode mismatch in a linear optics quantum gate. *New Journal of Physics*, 13(5):053036, 2011.

[25] Hossein Rouzegar and Mohammad Ghanbarisabagh. Estimation of doppler curve for leo satellites. *Wireless Personal Communications*, 108(4):2195–2212, 2019.

[26] Anthony E Siegman. *Lasers*. University science books, 1986.

[27] Orazio Svelto, David C Hanna, et al. *Principles of lasers*, volume 1. Springer, 2010.

[28] Thorlabs. Photodetectors. https://www.thorlabs.com/navigation.cfm?guide_id=36.

[29] Thorlabs. Polarizing Beamsplitters. https://www.thorlabs.com/navigation.cfm?guide_id=2224.

[30] Dmytro Vasylyev, W Vogel, and Florian Moll. Satellite-mediated quantum atmospheric links. *Physical Review A*, 99(5):053830, 2019.